ELSEVIER

Available online at www.sciencedirect.com

SCIENCE DIRECT®

Journal of Crystal Growth 269 (2004) 10–14

JOURNAL OF CRYSTAL GROWTH

www.elsevier.com/locate/jcrysgro

Ultrafast carrier dynamics in InN epilayers

Fei Chen[a], A.N. Cartwright[a,*], Hai Lu[b], William J. Schaff[b]

[a] Department of Electrical Engineering, 332 Bonner Hall, University at Buffalo, NY 14260, USA

[b] Department of Electrical and Computer Engineering, Cornell University, Ithaca, NY 14853, USA

Abstract

Ultrafast differential transmission measurements on a series of InN epilayers, grown by molecular beam epitaxy, have been employed to determine the carrier lifetimes and to probe the carrier recombination dynamics at room temperature. Differential transmission spectra reveal a peak energy of $\sim$0.7 eV on these samples, supporting the existence of the narrow band gap of InN. In addition, we observed a fast initial hot carrier cooling followed by a slow recombination process after pulse excitation. Carrier lifetimes ranging from 48 ps to 1.3 ns have been measured in these samples. An inverse proportionality between the carrier lifetime and the free-electron concentration was observed, suggesting that the donor-like defects or impurities may stimulate a formation of non-radiative recombination centers, reducing the carrier lifetime.

© 2004 Elsevier B.V. All rights reserved.

PACS: 78.47.+p; 71.35.−y

Keywords: A1. Optical properties; A1. Time-resolved spectroscopy

InN is the least studied of the III-nitride materials due to the difficulties encountered in the growth of compounds with large size differences between cation and anion, as well as its low thermal stability. Recent significant progress in growth techniques has led to the availability of high crystalline quality hexagonal InN layers with low free-electron concentrations [1–3]. Surprisingly, the optical characterization of these improved wurtzite InN crystals, although still a subject of debate, has provided convincing evidence that there is a band edge around 0.7–0.9 eV [4–7], much narrower than the $\sim$1.9 eV that was measured in earlier studies of InN [8,9]. This unexpected discovery has provided new opportunities for potential applications of InN based optoelectronic devices, such as infrared emitters.

In spite of important recent developments on the measurement and calculation [10,11] of the physical and optical properties of narrow gap InN, the carrier recombination dynamics and the associated carrier lifetimes are still unknown. There is no doubt that the understanding of carrier recombination mechanisms and the measurement of carrier lifetime are important in designing and optimizing InN based devices, as well as in optimizing material growth conditions. In this article, we report the carrier dynamics study and carrier lifetime measurements on a series of

*Corresponding author. Tel.: 1-716-645-3115x1205.
E-mail address: anc@eng.buffalo.edu (A.N. Cartwright).

0022-0248/$ - see front matter © 2004 Elsevier B.V. All rights reserved.
doi:10.1016/j.jcrysgro.2004.05.028

InN epilayers. Carrier lifetimes ranging from 48 ps to 1.3 ns have been obtained and show an inverse proportionality to the free-electron concentrations for these samples. This inverse proportionality suggests that the donor-like defects or impurities stimulate the formation of non-radiative recombination centers, reducing the carrier lifetime.

Four unintentionally doped InN films were grown on (0 0 0 1) sapphire with different buffer layers by molecular beam epitaxy. The details of the growth technique have been reported elsewhere [2]. The structures contain (i) sample A, GaN(220 nm)/InN(600 nm); (ii) sample B, AlN(300 nm)/InN(350 nm); (iii) sample C, GaN(220 nm)/InN(850 nm); and (iv) sample D, GaN(300 nm)/$In_{0.65}Ga_{0.35}N$(110 nm)/InN(7500 nm). X-ray diffraction studies show that these are high-quality wurtzite structured InN epitaxial layers formed with their *c*-axis perpendicular to the substrate surface. The mobility and free-electron concentration were measured at room temperature as $826\,cm^2/V\,s$ and $1.2\times10^{19}\,cm^{-3}$ for sample A, $820\,cm^2/V\,s$ and $2.7\times10^{18}\,cm^{-3}$ for sample B, $1340\,cm^2/V\,s$ and $1.3\times10^{18}\,cm^{-3}$ for sample C, and $2050\,cm^2/V\,s$ and $0.4\times10^{18}\,cm^{-3}$ for sample D, respectively.

Time-resolved differential transmission (transmission type pump/probe) measurements were performed at room temperature using a Coherent regenerative amplifier (REGA), operating at 250 kHz. The output of the REGA was frequency doubled to 400 nm to serve as the pump source for an optical parametric amplifier that generates a tunable infrared pulse (0.9–3.6 μm) with typical pulse widths of ~300 fs. In these experiments, the tunable infrared pulse was used as the probe beam and the remaining output of REGA at 800 nm served as the pump beam. Continuous-wave photoluminescence (PL) spectroscopy was also performed on these samples by using an Ar^+ laser with a photon energy of 3.41 eV.

The typical PL spectra at 20 K (solid line) and 300 K (dotted line), and the absorption spectra (dashed line) at room temperature for these samples are illustrated in Fig. 1. Consistent with the recent measurements [4], both PL peak energy and absorption edge coincide at ~0.7 eV. (Due to the band gap of $In_{0.65}Ga_{0.35}N$ buffer layer and the thickness of InN layer for sample D, only a short wavelength range of absorption spectra was taken on this sample.) Not surprisingly, we also observed that the emission width and band edge increases with increasing free-electron concentration, indicating the transitions from high energy states in the conduction band contribute significantly to the PL spectra. In addition, the functional form of the absorption coefficient above the band edge can be well described by $(E-E_g)^{1/2}$ for all the samples, which indicates a direct interband transition.

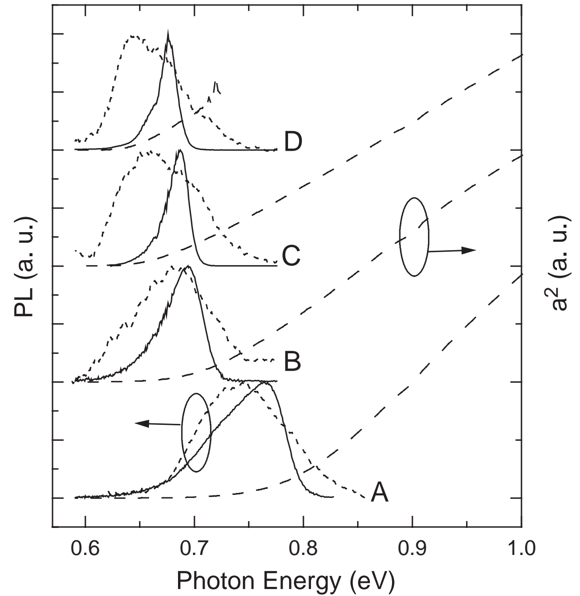

Fig. 1. PL spectra taken at 20 K (solid line) and room temperature (dotted line), and room temperature absorption coefficient squared (dashed line) for all the samples.

In the time-resolved differential transmission measurements, each intense 800 nm pump pulse injects free carriers much higher into the bands of InN, creating a dense and hot carrier distribution initially localized near the pump energy. After pulse excitation, the non-thermalized photoexcited carriers interact mostly through carrier–carrier scattering, and reach a thermalized distribution at a carrier temperature higher than the lattice temperature within the time scale of ~100 fs. Due to the relatively broad pulse width of our laser systems, this process cannot be monitored. The thermalized hot carriers then, initially at a

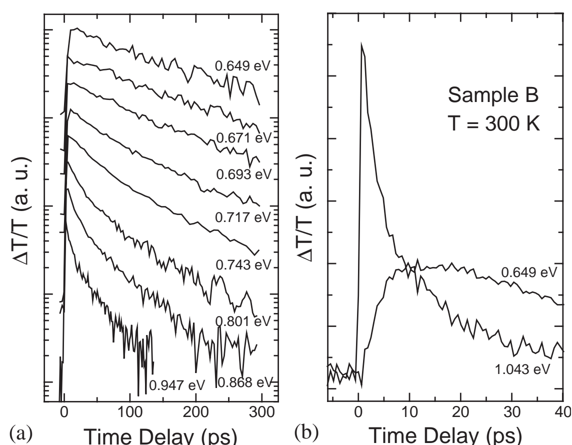

Fig. 2. (a) Strength of the differential transmission signal vs. time delay for different photon energies, and (b) differential transmission signals at short times for photon energies of 0.649 and 1.043 eV on sample B under a pump fluence of 120 μJ/cm^2 at room temperature.

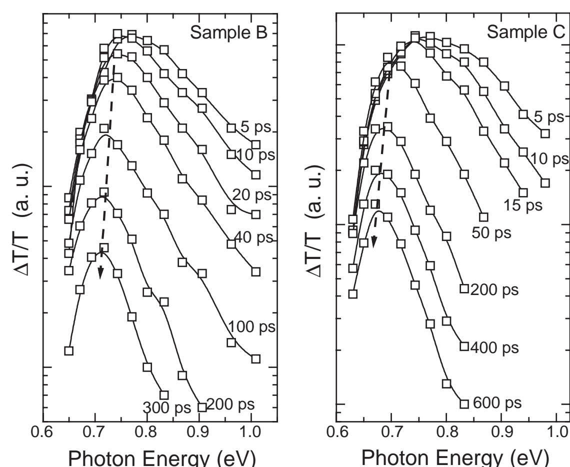

Fig. 3. Differential transmission spectra as a function of time delay (a) on sample B and (b) on sample C under a pump fluence of 120 μJ/cm^2 at room temperature.

temperature higher than the lattice temperature, transfer energy to the lattice and reach equilibrium through phonon emission. Fig. 2(a) shows the measured differential transmission signal as a function of time delay on sample B under a fixed pump fluence of 120 μJ/cm^2 at various probed photon energies. The instantaneous increase in the probe transmission near zero time delay is the result of phase space filling induced by the pump pulse. The signal at low energies decays single exponentially with time. In contrast, for high energies the signal shows an initial fast decay followed by a slower relaxation. The fast decay component at short times results from hot carrier cooling, while the slow decay component is attributed to the carrier recombination process. To explore the hot carrier cooling effect, we also plot the differential transmission signal at very short times. An observed fast decay at an energy of 1.043 eV and a slight increase with time at an energy of 0.649 eV are presented in Fig. 2(b), and it reflects the relaxation of hot carriers from higher energy states to lower energy states.

Fig. 3 illustrates the differential transmission spectra at different time delays for sample B and sample C. The arrows in the figure indicate the spectral peak positions versus times. Consistent with the PL and absorption measurements, differential transmission spectra with a peak energy of ~0.7 eV were observed and further verify the existence of a narrow band gap in InN. It is also interesting to note that at the shortest time delay, the spectrum is broad. As the time delay is increased, the spectra become narrower indicating relaxation of the hot photoexcited carriers, and the high-energy tail becomes steeper indicating a decrease in the carrier temperature [12,13]. More importantly, Fig. 3 shows that the peak energy of differential transmission spectra redshifts with time, which is consistent with a reduction of the bandfilling effect as the photoexcited carriers recombine.

Fig. 4 shows the measured differential transmission signal, with a probe energy set corresponding to the PL peak energy for each sample, as a function of time delay under a fixed pump fluence of 120 μJ/cm^2. The absorption recovery is close to a single exponential for all four samples and the carrier lifetimes derived from the curves vary from 48 ps (sample A), 150 ps (sample B), 520 ps (sample C), to 1.3 ns (sample D) by an exponential fit. For the samples investigated here, our results demonstrate that carrier lifetime is almost inversely proportional to the free-electron concentration, thus a linear curve can be obtained when plotting the carrier lifetime versus free-electron

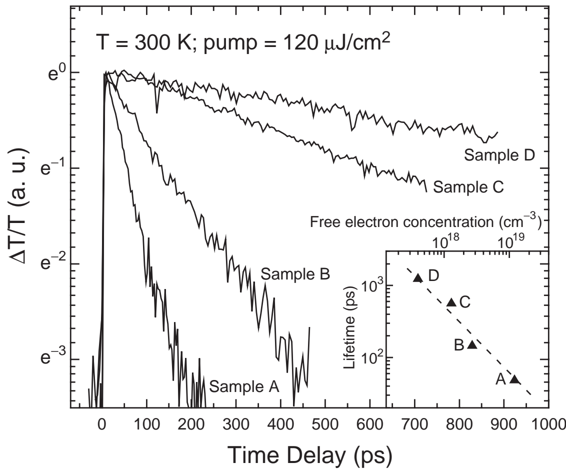

Fig. 4. Strength of the differential transmission signal vs. time delay under a pump fluence of $120\,\mu J/cm^2$ at room temperature. The inset graph shows the carrier lifetime as a function of free electron concentration.

concentration on a log–log scale (inset of Fig. 4). A significant reduction in carrier lifetime due to the increase of free-electron concentration is obvious here. In terms of device design and optimization, this relationship may be used to estimate the carrier lifetime by measuring the free-electron concentration.

It is well known that the recombination of the photogenerated carriers follows three different channels: non-radiative defect-related, bimolecular radiative interband, and non-radiative Auger. Thus, the carrier lifetime is described by

$$\frac{1}{\tau} = \frac{1}{\tau_{nr}} + B(n + n_0) + C(n + n_0)^2,$$

where B and C are interband and Auger recombination coefficients, τ_{nr} is the non-radiative lifetime, n is the photogenerated carrier density, and n_0 represents the free-electron concentration. The above equation implies that, for radiative and Auger recombinations, the lifetime has a carrier density dependent characteristic which results in a non-exponential decay. On the contrary, the defect-related non-radiative lifetime, depending on the defect density, is independent of photogenerated carrier density. Under a pump fluence of $120\,\mu J/cm^2$, the corresponding average photoexcited carrier density is estimated as $2.8 \times 10^{18}\,cm^{-3}$, which is of the same order or higher than the free-electron concentration in each sample. Hence, the single exponential decay for all the samples is consistent with the trapping of photogenerated carriers by defects or impurities, resulting in the fast non-radiative recombination.

To further elucidate the nature of recombination in these samples, the carrier lifetimes were also measured as a function of photogenerated carrier density by varying the pump fluence from 60 to $480\,\mu J/cm^2$. The general behavior for all the samples is the same: as the pump fluence is increased, even in the case where the photogenerated carrier density is sufficiently higher than the free-electron concentration, the decay curves still remain a single exponential and there is no observable change in carrier lifetime. Thus, these results further support our assumption that the defect-related non-radiative recombination plays a dominant role in the carrier recombination process in these InN epilayers at room temperature.

Another important feature we have mentioned earlier is the inverse proportionality between the carrier lifetime and the free-electron concentration. These donors in the unintentionally doped InN have not yet been identified, but potential candidates have been attributed to nitrogen vacancy or antisite [8,14], the oxygen and silicon impurities [15], or hydrogen impurities [16]. Let us remember the non-radiative lifetime τ_{nr} is related to the defect density N_{defect} by the following expression: $1/\tau_{nr} = \sigma \upsilon N_{defect}$, where σ is the carrier capture cross section and υ represents the carrier velocity. Obviously, it is reasonable to assume that the donor-like defects or impurities, not only provide free electrons, but may also stimulate the formation of (or work as) the non-radiative recombination centers, reducing the carrier lifetime.

In summary, ultrafast differential transmission measurements were performed to probe the carrier recombination dynamics in InN epilayers. We have observed a fast hot carrier cooling followed by a slow recombination process after pulse excitation. Carrier lifetimes as long as 1.3 ns have been observed. Our results indicate that the defect-related non-radiative recombination process is

dominant in these samples at room temperature. Furthermore, an inverse proportionality between the carrier lifetime and the free-electron concentration was found and suggests that the donor-like defects or impurities may stimulate a formation of non-radiative recombination centers.

This work was supported by the National Science Foundation CAREER Award, NSF No. 9733720, under the direction of Dr. Filbert Bartoli, and the Office of Naval Research Young Investigator Program Award No. N00014-00-1-0508 under the direction of Dr. Colin Wood.

References

[1] V.V. Mamutin, A.A. Vekshin, V.Y. Davydov, V.V. Ratnikov, T.V. Shubina, S.V. Ivanov, P.S. Kopev, M. Karlsteen, U. Soderwall, M. Willander, Phys. Stat. Sol. (a) 176 (1999) 247.
[2] H. Lu, W.J. Schaff, J. Hwang, H. Wu, W. Yeo, A. Pharkya, L.F. Eastman, Appl. Phys. Lett. 77 (2000) 2548.
[3] Y. Saito, N. Teraguchi, A. Suzuki, T. Araki, Y. Nanishi, Jpn. J. Appl. Phys. Part 2 40 (2001) L91.
[4] J. Wu, W. Walukiewicz, K.M. Yu, J.W. Ager III, E.E. Haller, H. Lu, W.J. Schaff, Y. Saito, Y. Nanishi, Appl. Phys. Lett. 80 (2002) 3967.
[5] T. Matsuoka, H. Okamoto, M. Nakao, H. Harima, E. Kurimoto, Appl. Phys. Lett. 81 (2002) 1246.
[6] V.Y. Davydov, A.A. Klochikhin, R.P. Seisyan, V.V. Emtsev, S.V. Ivanov, F. Bechstedt, J. Furthmuller, H. Harima, A.V. Mudryi, J. Aderhold, O. Semchinova, J. Graul, Phys. Stat. Sol. B 229 (2002) R1.
[7] J. Wu, W. Walukiewicz, W. Shan, K.M. Yu, J.W. Ager III, E.E. Haller, H. Lu, W.J. Schaff, Phys. Rev. B 66 (2002) 201403.
[8] T.L. Tansley, C.P. Foley, J. Appl. Phys. 59 (1986) 3241.
[9] Q. Guo, A. Yoshida, Jpn. J. Appl. Phys. 33 (1994) 2453.
[10] F. Bechstedt, J. Furthmuller, J. Crystal Growth 246 (2002) 315.
[11] S. Wei, X. Nie, I.G. Batyrev, S.B. Zhang, Phys. Rev. B 67 (2003) 165209.
[12] K. Kash, J. Shah, Appl. Phys. Lett. 45 (1984) 401.
[13] K. Kash, D. Block, J. Shah, Phys. Rev. B 33 (1986) 8762.
[14] M. Sato, Jpn. J. Appl. Phys. Part 2 36 (1997) L658.
[15] C. Stampfl, C.G. Van de Walle, D. Vogel, P. Kruger, J. Pollmann, Phys. Rev. B 61 (2000) R7846.
[16] D.C. Look, H. Lu, W.J. Schaff, J. Jasinski, Z. Liliental-Webber, Appl. Phys. Lett. 80 (2002) 258.